RESEARCH ARTICLE Received: 16 May 2019 | Accepted: 11 June 2019 | Online: 12 July 2019

JOURNAL OF GEOPHYSICS
Est. 1924
www.geophysicsjournal.com

Tomographic imaging of the Andravida blind strike-slip fault (Western Greece)

A. Karakonstantis[1*], K. Pavlou[1], V. Kapetanidis[1]

[1)] Department of Geophysics-Geothermics
National and Kapodistrian University of Athens
Panepistimiopolis, Zografou 15784, Greece

On 8 June 2008 at 12:25 GMT, a large (M_w6.4) earthquake occurred NE of the town of Andravida in Western Peloponnese, Greece – an area characterized by high seismicity during the last decade. In this study, the local velocity structure of the Andravida Fault Zone (AFZ) is investigated primarily using data recorded during the period 2012-2017 by the Hellenic Unified Seismological Network (HUSN). We selected about 1,500 seismic events recorded by the local HUSN stations as well as the Hellenic Strong-Motion Network (HSMN). By applying tomographic inversion, we produced and interpreted 3D models of V_P, V_S, and V_P/V_S ratio in the study area. The spatial distribution of the aftershocks, as well as the 3D model derived by Local Earthquake Tomography (LET), provided evidence for the rupture plane. Surface breaks and minor faults are found to be oblique to the main direction of the AFZ, as a result of a restraining bend in Mtn. Movri and the formation of a positive flower-structure in the shallow layers of the upper crust.

Key words—Andravida earthquake, Western Greece, travel-time tomography, restraining bend.

1. Introduction

Greece is located in the eastern end of Europe where a variety of geological processes – such as the Alpine orogenesis – take place. The creation of the Alpine mountain chain, as one of the most important geological features, is caused by the collision between Europe and Africa. Furthermore, intense deformation observed in Greece and surrounding areas produces significant seismicity concentrated in certain seismic zones, such as the Hellenic Arc. This seismicity consists of thrust tectonics, strike-slip faulting, as well as normal faults in the back-arc area (Papazachos and Papazachou, 1997; Aksu et al., 2000).

The region of western Greece (Fig. 1) is characterized by complex tectonics that involves a compressional stress field along the Hellenic Arc, and an extensional one in the back-arc area with the Corinth Rift as the major structure. The dynamics of the convergent plate boundaries dramatically change from NW to SW Greece (Kassaras et al., 2016). The region of the Greek-Albanian border is dominated by a continent-continent collision, expressed mainly by reverse focal mechanisms, with a deformation rate of up to about 100 nstrain/yr (Hollenstein et al., 2008). South of Zakynthos Island, the geodynamic regime is totally changed to ocean-continent subduction, characterized by thrust faulting along the Hellenic Arc, with GPS velocities of approximately 20 mm/yr (Hollenstein et al., 2008). The transition zone between the collision zone to the North, and the subduction zone to the South, is characterized by the Cephalonia-Lefkas Transform Fault Zone (CLTFZ) (Papadimitriou et al., 2006) – exhibiting dextral strike-slip faulting with a deformation rate of about 10 mm/yr (Kahle et al., 1995; Lagios et al., 2007; Chousianitis, 2010). This differentiation of the geodynamic regime is expressed both by the GPS-derived velocities and the increase of seismicity towards the south in western Greece.

The main feature of the back-arc region is the Corinth Gulf, located in central Greece east of Cephalonia Island. The gulf is dominated by normal faults striking E-W and by N-S extension (Armijo et al., 1996; Papadimitriou et al., 2010a). The regime is gradually changing towards NW where Trichonis Lake is situated. In this region both the NW-SE normal and the strike-slip faulting, are observed. The tectonic setting also changes towards south Peloponnese, where normal faulting in the N-S direction, and the E-W extension, are observed due to a 90° rotation of the stress field about the vertical S1 maximum principal stress axis (Kapetanidis & Kassaras, 2019). Western Peloponnese (Fig. 2) is mainly composed of Alpine sedimentary rocks of the Gavrovo and Pindos geotectonic units. The whole unit is intensively folded and faulted, forming successive thrusts of Mesozoic and early Cenozoic age, which are cut by normal neotectonic faults. On the other hand, SW Peloponnese is characterized by the presence of neotectonic (post-Miocene) structures, including large grabens and horsts bounded by wide fault zones that strike both N-S and E-W. The pattern and growth of these neotectonic units are complicated because of regional uplift, crustal block rotation, and normal fault development throughout the Quaternary; see, e.g., Armijo et al. (1992).

[*)] Correspondence to: akarakon@geol.uoa.gr.

ARK:https://n2t.net/ark:/88439/x014750 2643-9271/19/63/0001/0014

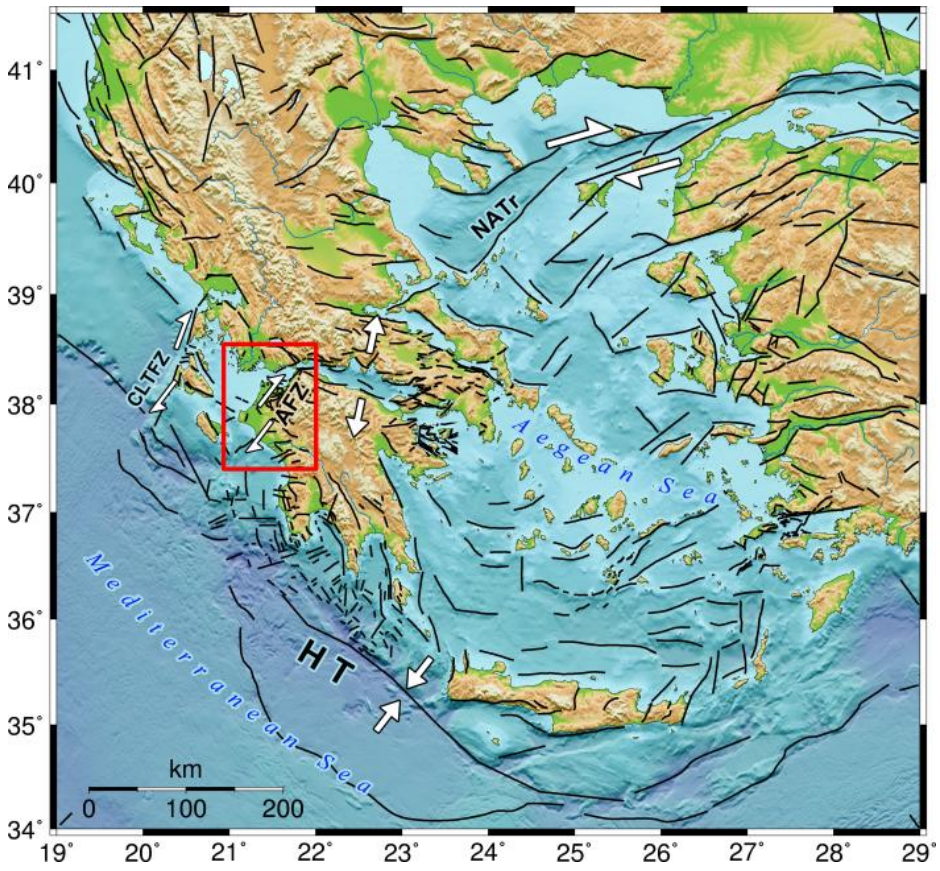

Figure 1. Main tectonic features in Greece and Western Turkey. Abbreviations-AFZ: Andravida Fault Zone; HT: Hellenic Trench; NATr: North Aegean Trough. Fault traces derived by Pavlidis et al. (2010) and Ganas et al. (2013).

2. SEISMICITY

The region – as shown on Fig. 2 and delineated by the Ionian Islands of Lefkas, Cephalonia, and Zakynthos to the west, the city of Aigio in the Corinth Gulf to the east, the Amvrakikos Gulf to the north and Pyrgos city in Western Peloponnese to the south – is characterized by a very low background-seismicity, possibly defining a "nano-plate" also known as Cephalonia-Lefkas-Aitoloakarnania Block (CLAB) (Kassaras et at., 2016). The tectonics in Western Peloponnese is unclear due to the lack of major surface fault-escarpments, and the absence of large historical earthquakes. Moderate seismic activity in the area was expressed by the 16 October 1988 event (M_w5.8) which caused some damages in the town of Vartholomio, as well as by the 7 June 1989 (M_w5.2), the 26 March 1993 Pyrgos (M_w5.5) and the 14 July 1993 Patras events (M_w5.6) (Koukouvelas et al., 1996; Tselentis, 1998; Lekkas et al., 2000) which occurred at the distance of 14 km, 45 km and 27 km from the Andravida event, respectively. During the 1990s, seismic activity has significantly increased in the broader area of Western Peloponnese, with the most important events being the Vartholomio of December 2002 (Roumelioti et al., 2004), the Zakynthos of April 2006 (Papadimitriou et al., 2010b), the Trichonis of April 2007 (Kiratzi et al., 2008; Kassaras et al., 2014), and the Chalandritsa of February 2008 (Kapetanidis et al., 2010) earthquake sequences.

A large (M_w6.4) dextral strike-slip earthquake occurred on 8 June 2008 at about 22 km E-NE of Andravida town in the Western Peloponnese, in an area where seismicity remained remarkably low during the instrumental period. More specifically, the epicenter was at 7 km NE of the artificial Pinios Lake and 38 km SW of the city of Patras. Despite a large magnitude of this event, no co-seismic rupture of the activated fault was observed in the vicinity of the epicenter. However, secondary ground fissures were reported in a broader area, at: Nisi (trending almost NNW–SSE), Vithoulkas (trending generally N–S), and Michoi (trending WNW–ESE) (Koukouvelas et al., 2010). Furthermore, railway tracks were strongly deformed in Kato Achaia (Mavroulis et al., 2010), the meizoseismal area with the highest macroseismic intensity, which, notably, does not coincide with the epicentral area and is situated at approximately 20 km NE of the mainshock's location. The seismic activity remained at relatively high levels during the study period (2012-2017), accommodated along the NE-SW dextral strike-slip fault zone, as seen in Fig. 3.

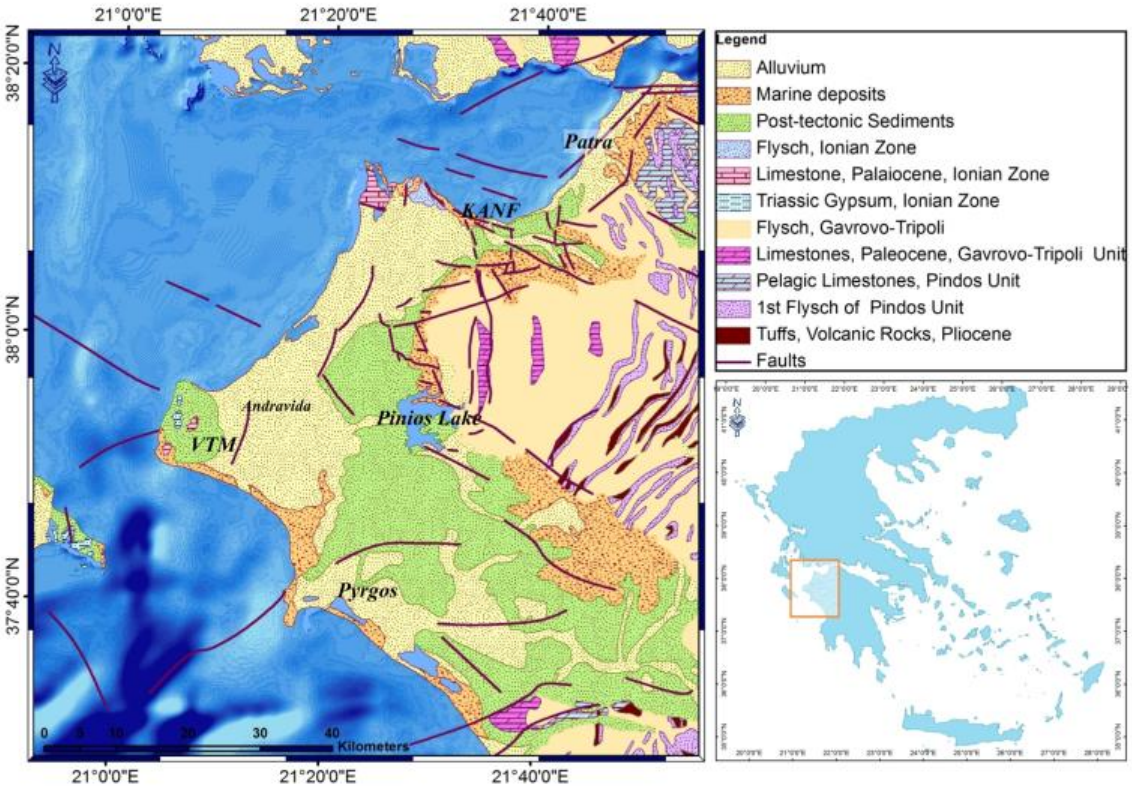

Figure 2. Geological features in the area of study (Western Peloponnese). Abbreviations- KANF: Kato Achaia Normal Fault; VTM: Vartholomio. Main geologic and tectonic elements derived by Koukouvelas et al. (2009), Pavlidis et al. (2010) and Ganas et al. (2013).

3. Data and Algorithm

The goal of this tomographic study was to determine the crustal structure in the Western Peloponnese in order to identify the blind fault that was ruptured during the 2008 Andravida earthquake sequence, utilizing manually located events. LET techniques have been successfully applied to reveal the velocity structure in such cases (e.g., Drakatos et al., 2002; Koulakov et al., 2010). In the present study, the analysis was based on the LOcal TOmographic Software (LOTOS) by Koulakov (2009).

P- and S-phases of more than 1,500 events recorded during 2012-2017 by stations of the Hellenic Unified Seismological Network (HUSN) and the Hellenic Strong-Motion Network (HSMN), located in Central Greece, were used for the tomographic inversion. Synthetic tests were performed to set the input parameter values that produced better resolution and increased the fidelity area. For the 3D tomographic inversion, a dataset consisting of 44,417 P- and 22,541 S-arrival-times was selected, with at least 12 phases per event (Fig. 4). The algorithm provides two alternative options: inversion for V_P and V_S (V_P–V_S scheme) using P and S travel-time residuals (dt_P and dt_S), and inversion for V_P and V_P/V_S ratio (V_P–V_P/V_S scheme) using dt_P and differential residuals, $dt_S - dt_P$. In order to obtain additional constraints on the V_P and V_S anomalies, the inversion was performed in this study for both V_P–V_S and V_P–V_P/V_S schemes (Koulakov, 2009; Jaxybulatov et al., 2011).

For input data, we used the stations' coordinates, their elevations, and the arrival times from locally recorded seismicity. Coordinates of the hypocenters and the origin times are not required since determined along with the computations. However, if preliminary hypocentral locations are available, as in the present case, they are used to decrease the processing time. Additionally, the available initial 1–D velocity model (Karakonstantis, 2017) and a set of input parameters to perform the convergence iteration steps, i.e., parameterization, grid dimensions, and damping parameter, are defined by the user (Koulakov 2009). We employed a nodal representation, given that the velocity field, reconstructed by a three-dimensional grid, does not assume a specific geometry of heterogeneities (Toomey and Foulger, 1989). The grid spacing (~2 km) was kept considerably smaller than the expected resolution length, to reduce the bias of the resulting models due to the grid configuration. The optimal grid mesh was determined while taking into account the stations/events geometry. In addition, to further decrease the influence of the model parameterization on the solutions, the inversion was repeated using four grid orientations (0˚, 22˚, 45˚, and 67˚). The inversion results, obtained for the previously mentioned grids, were stacked into one summary model, reducing the artifacts related to grid orientation, as described by Koulakov (2009).

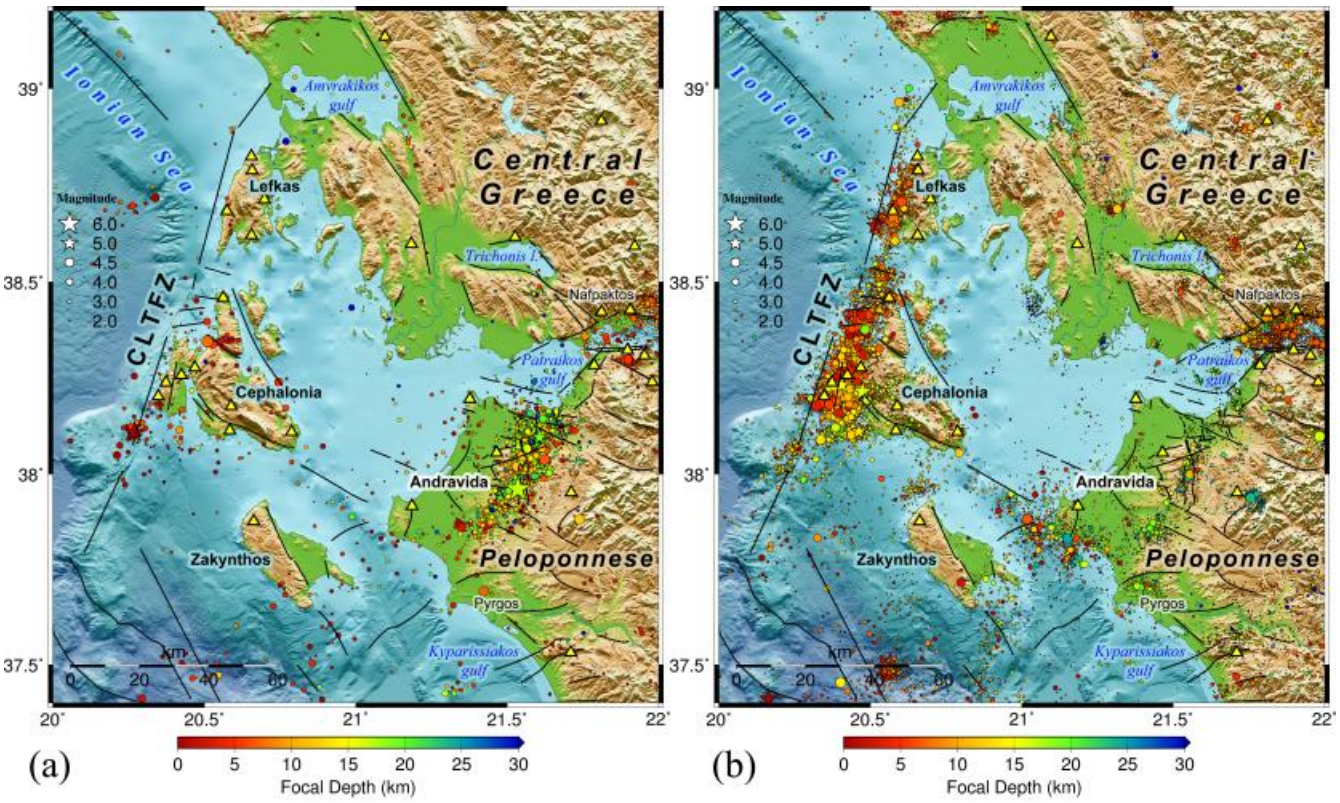

Figure 3. Seismic activity in the broader area of study a) for the period between June-August 31, 2008, including the aftershocks of the Mw6.4 Andravida earthquake of June 8th, 2008, and b) for the 2012-2017 period. Yellow triangles are the available local stations of HUSN and HSMN.

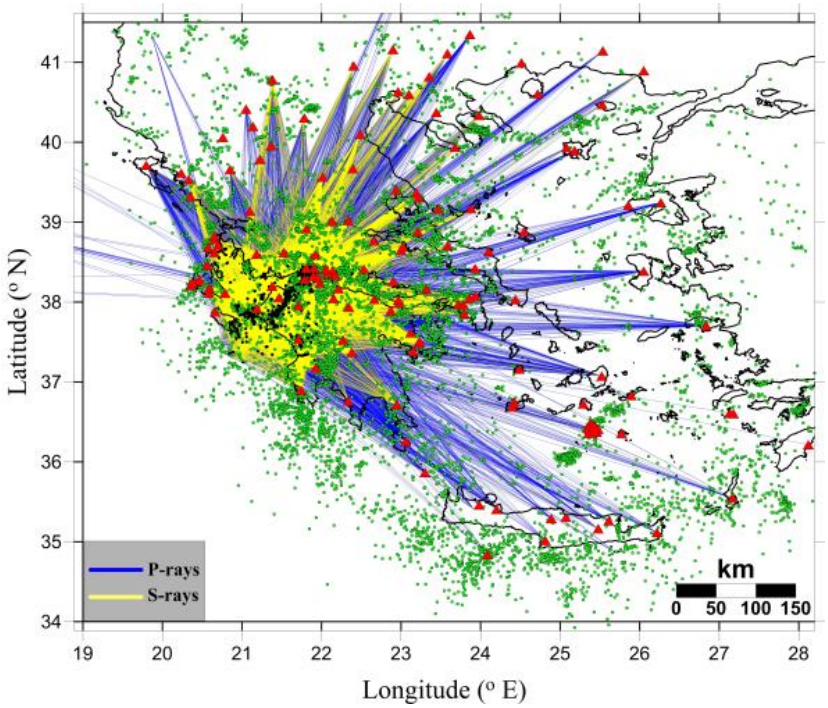

Figure 4. Total P- (blue) and S-ray (yellow) distribution. Red triangles indicate locations of the HUSN and the HSMN stations. The background seismicity (M ≥ 2.8) during 2012-2017 is presented by green and the selected seismicity in the study area by black circles (Karakonstantis, 2017).

V_P/V_S ratio	1.79	
Layer	P-wave Velocity (km/s)	Ceiling Depth (km)
1	4.9	0.0
2	5.8	2.5
3	6.1	8.5
4	6.4	17.0
5	6.9	21.0
6	7.0	24.0
7	7.3	35.0

Table 1. The 1-D velocity model (Karakonstantis, 2017) used in this study.

4. RESULTS

4.1 Sensitivity analysis

A sensitivity analysis for the available dataset was performed using the checkerboard test (Humphreys and Clayton, 1988). This method uses alternating anomalies of fast and slow velocity perturbations, relative to the initial 1-D gradient model, evenly spaced throughout the model in a checkerboard pattern (Fig. 5). The data resolution is mainly controlled by the ray-path distribution, by the model parameterization, and by smoothing (Lees and Crosson, 1989). The average spacing between stations is of the same order as the minimum size of the resolved anomalies in the tomographic inversion (Koulakov and Shapiro, 2015).

Checkerboard tests are performed to reproduce the attributes of the real-data-processing procedure. In the initial synthetic models, the cell size corresponds to the expected anomalies. The applied procedure requires the definition of spiked regions, with a 10% variability in the velocity structure, compared to the reference 1-D velocity model; see Table 1. We first compute travel-times for the paths between the source and the receiver. Subsequently, we add random noise to synthetic travel-time residuals to resemble the respective RMS errors of 0.15 s for P-waves and 0.25 s for S-waves observed in the real data. This procedure corresponds to a real observation system that uses 3D ray tracing that follows the bending algorithm principles.

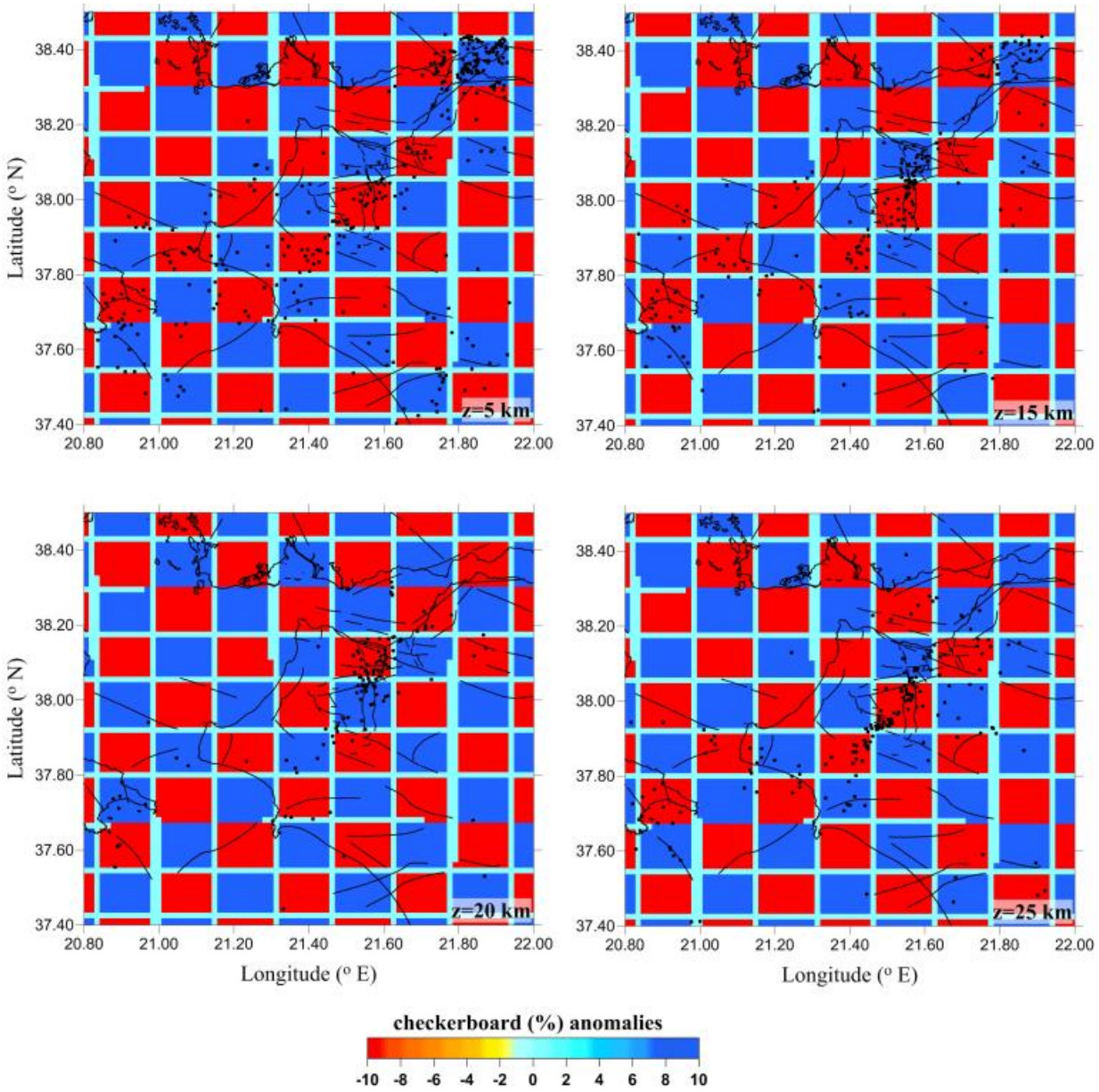

Figure 5. Initial checkerboard model for the depth slices of 5, 15, 20, and 25 km, with the anomaly cell size of 7x7 km^2.

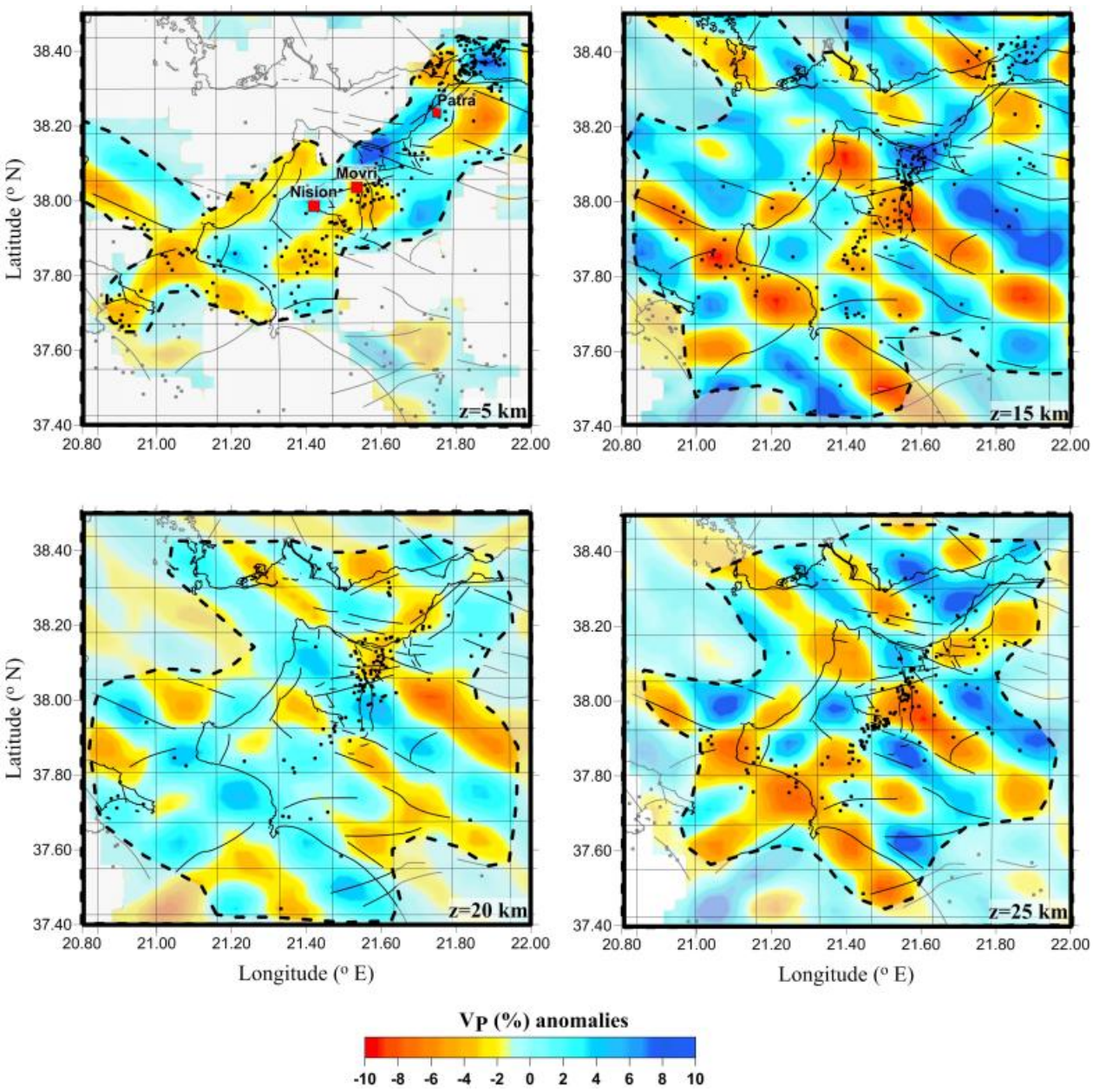

Figure 6. Reconstruction of P-wave anomalies for the depth slices of 5, 15, 20, and 25 km, with the anomaly cell size of 7x7 km^2. The confidence area is within the dashed-outline polygon.

We reconstructed the synthetic model in the same way as in the case of real data, including the 1-D velocity model optimazation and the absolute source location. After several synthetic-data tests, the set of parameters that provided a greater confidence area, and that could successfully reconstruct the model of checkerboard anomalies, was used for the 3D tomographic inversion of real data. Errors in the data control the inversion variance, and they include mis-picks, mislocations, and incorrectly determined ray-paths.

An example of a checkerboard test, presented herein, consists of alternating 7x7 km^2 anomalies for the horizontal tests, which were used to define the limitations of our model. The variations (in %) of body-wave velocity anomalies (± 10%) and the V_P/V_S ratio distribution, can be seen in Figs. 6-8, for depths of 5, 15, 20, and 25 km. The sign of the velocity was changed at the 5 km depth to check the vertical resolution. The synthetic model is reconstructed adequately within the region between the Pyrgos basin to the south and the southern shores of Central Greece near the city of Nafpaktos (37.7º-38.4ºN, 20.9º-22.0ºE). More specifically, the anomalies do not resolve well within the depth slice of 5 km depth for either of the P- and S-wave velocity models.

On the other hand, synthetic body-wave (P, S) anomalies were reasonably restored throughout the study area, in the depth slices for 15, 20, and 25 km depths (37.40ºN-38.45ºN, 20.85ºE-22.00ºE). Horizontal smearing was observed towards the NNE part of the study area and was mainly due to the azimuthal gap of the available seismological stations and the relatively sparse epicentral distribution. The synthetic tests have shown that the absolute amplitudes of the body-wave anomalies were up to 4% smaller than the respective amplitudes from the starting checkerboard grid.

These tests are used as a preliminary tool to understand whether the ray configuration enables the reconstruction of the shape of small patterns at all depths. In cases when this condition is not satisfied, the test results indicate the size of the anomaly preserved throughout the examined depth interval. The size and form of the resolved area for the horizontal slices, together with the presence of dense ray coverage for the horizontal slices, provide reliability to the interpretation of the final results of the velocity perturbations, as well as for the V_P/V_S values.

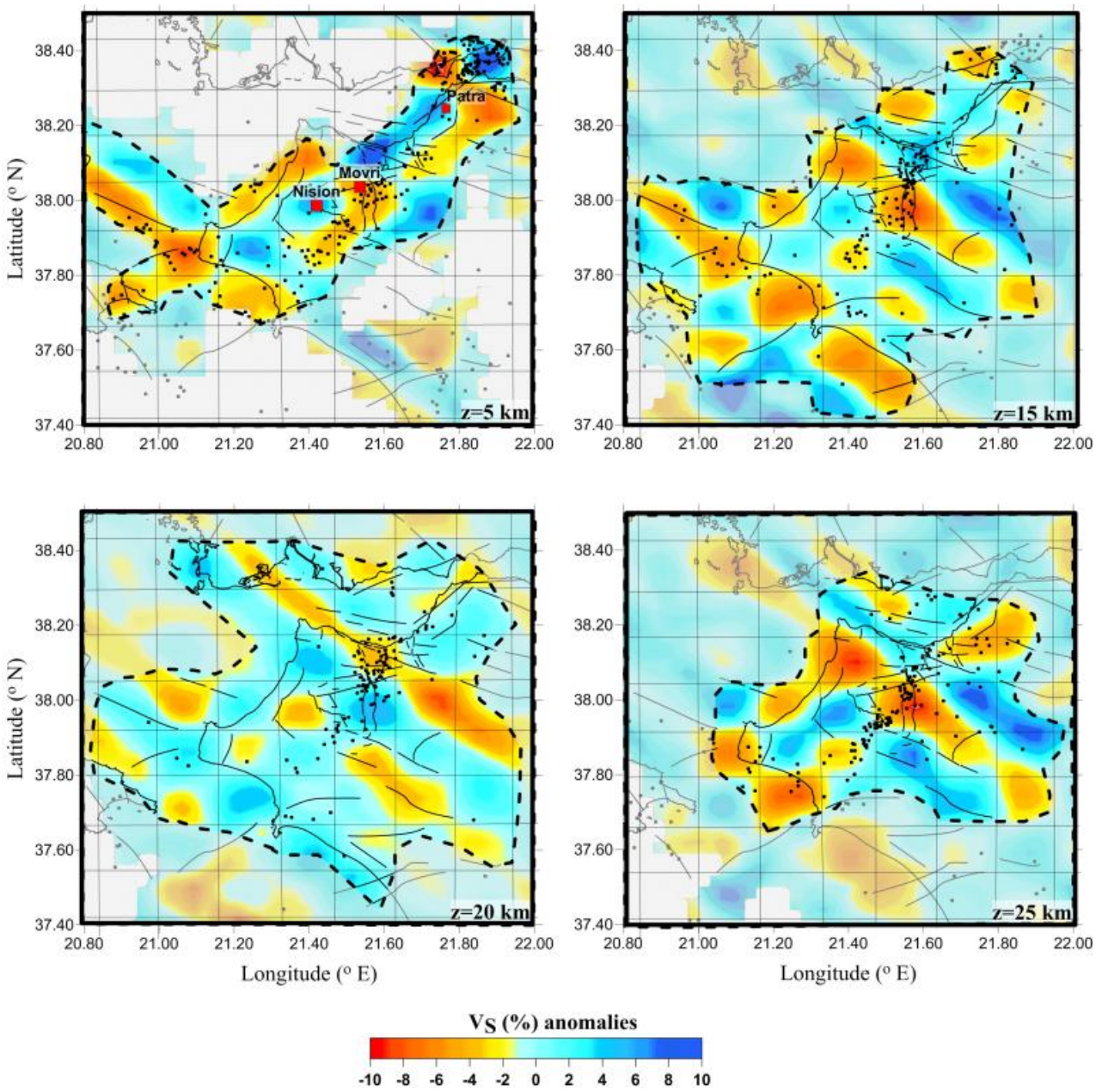

Figure 7. Reconstruction of S-wave anomalies for the depth slices of 5, 15, 20, and 25 km, with the anomaly cell size of 7x7 km^2. The confidence area is within the dashed-outline polygon.

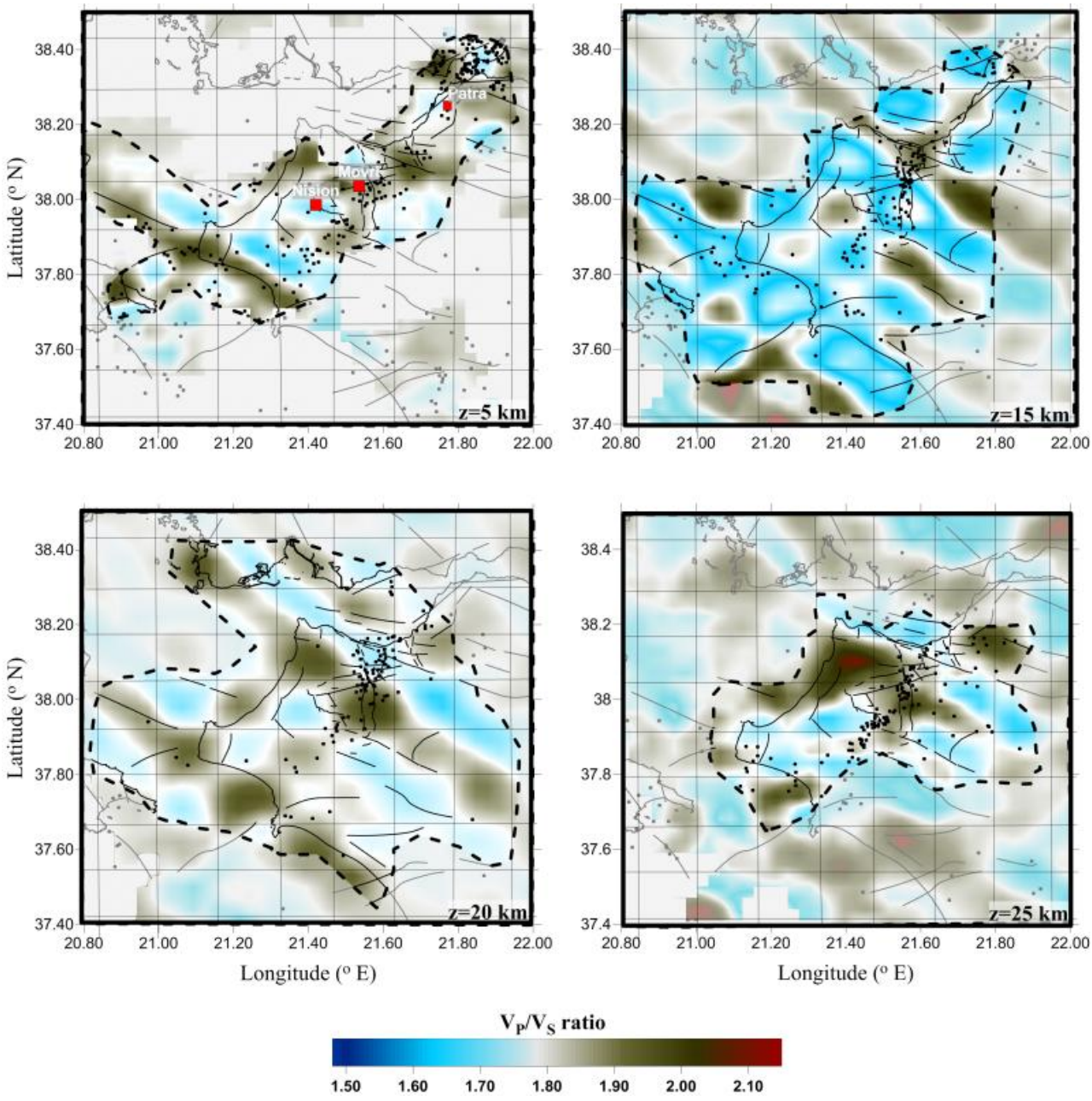

Figure 8. Reconstruction of S-wave anomalies for the depth slices of 5, 15, 20, and 25 km, with the anomaly cell size of 7x7 km^2. The confidence area is within the dashed-outline polygon.

4.2 Real-data inversion

The values of P- and S-wave residuals from different iteration steps of the inversion procedure are in Table 2. For the P- and S-data, the reduction of the residual is ~10% and 13%, respectively. The resulting P- and S-wave velocity anomalies with respect to the starting 1-D velocity model are shown in horizontal depth slices (Figs. 9-10). The interpretation of the obtained results is limited to the unmasked confidence regions as characterized by reasonable reconstruction of the checkerboard model. The mean computed P and S anomalies for the study area are within ±10%.

Strong NE-SW oriented negative velocity anomalies predominate at both the upper and the lower crust onshore the Peloponnese. In the tomograms of Figs 9-11, these anomalies are observed down to the 25 km depth west of Kyparissiakos Gulf and crossing central Peloponnese. At depths below 25 km, the model lacks resolution and can only be regarded indicative, hence it is not discussed here.

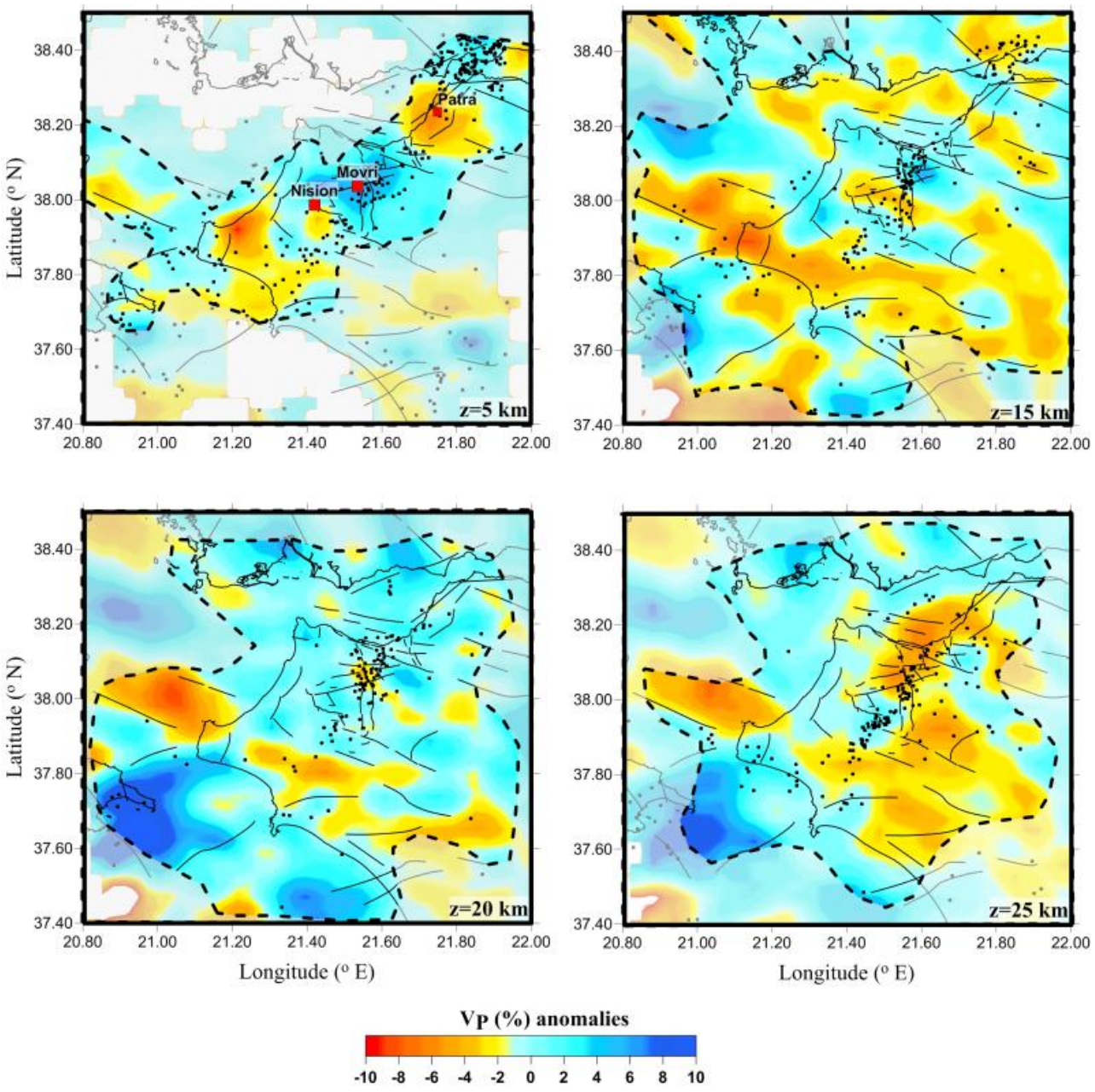

Figure 9. Tomograms of lateral VP (%) variations at 5, 15, 20, and 25 km depths. Areas with lower resolution are masked (darkened). Fault traces derived by Koukouvelas et al. (2009), Pavlidis et al. (2010), and Ganas et al. (2013).

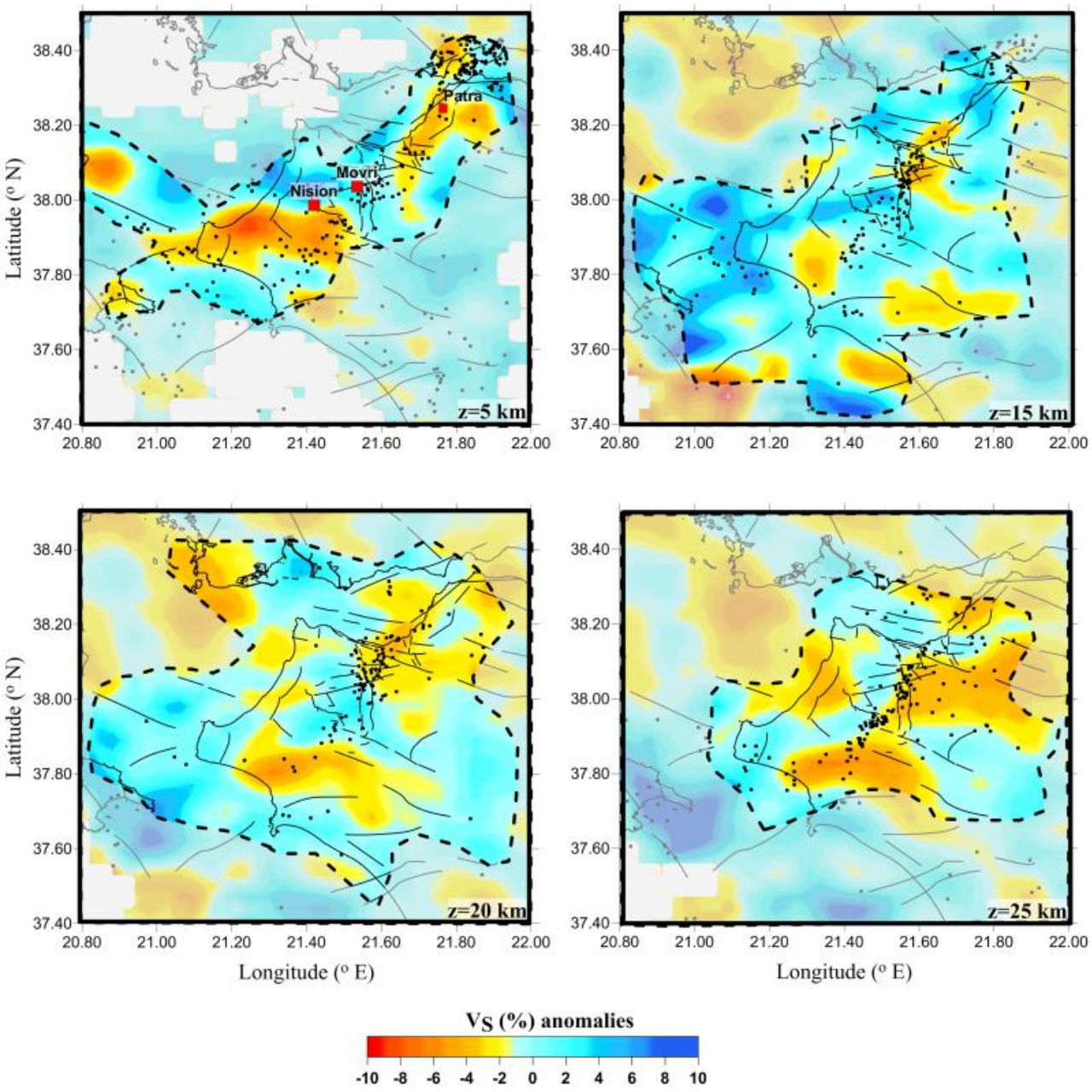

Figure 10. Tomograms of lateral V_S (%) variations at 5, 15, 20, and 25 km depths. Areas with lower resolution are masked (darkened). Fault traces derived by Koukouvelas et al. (2009), Pavlidis et al. (2010), and Ganas et al. (2013).

Iteration	P-residual (s)	P-residual reduction (%)	S-residual (s)	S-residual reduction (%)
1	0.262	0.00	0.427	0.00
2	0.244	7.06	0.387	9.41
3	0.239	8.93	0.376	12.06
4	0.237	9.50	0.372	12.76
5	0.236	9.98	0.369	13.40

Table 2. Average absolute values of P- and S-wave residuals and their cumulative reduction percentage during the inversion of synthetic data.

At the depth slice of 5 km, a NE-SW-trending zone of negative body-wave velocity perturbations and relatively low V_P/V_S ratio values (~1.70) appears near the city of Patras (Fig. 9-11). This anomaly follows the mean distribution of fluvial deposits and marine terraces of Pleistocene age which are bounded by positive (~6%) body-wave velocity perturbations and relatively high V_P/V_S ratio values (~1.92), possibly connected to the Mesozoic carbonate rocks to the east and the Agia Triada Fault (ATF) to the south, respectively (Koukouvelas et al., 2009).

An NW-SE-trending negative anomaly in P-waves is observed in the Patraikos Gulf north of Patras city, at the depth slice of 10 km. This anomaly coincides with the direction of the fault traces into the Gulf (Ferentinos et al., 1985). An approximately NNE-SSW discontinuity of positive-to-the-west and negative-to-the-east, body-wave (V_P and V_S) velocity anomalies (Figs. 9-10), is identified close to Mtn. Movri (south of Patras), in the depth slices of 20 and 25 km. This pattern is more distinct in the V_P/V_S ratio tomograms of the respective depth slices (Fig. 11). The distribution of both body-wave velocity anomalies and V_P/V_S ratio mark the trace of the northern branch of the activated fault (AFZ) during the 2008 Andravida earthquake (M_w6.4).

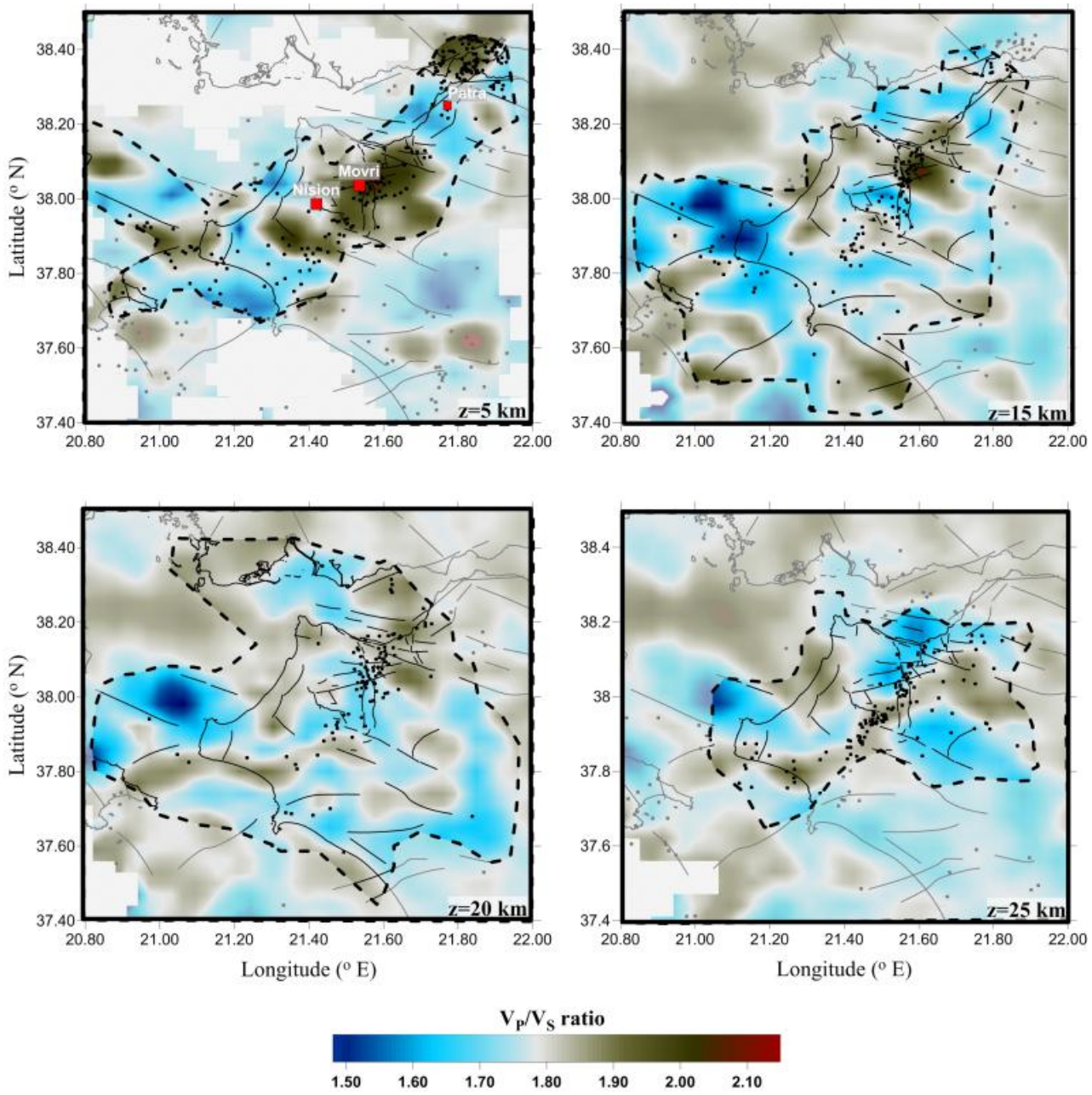

Figure 11. Tomograms of lateral V_P/V_S at 5, 15, 20, and 25 km depths. Areas with lower resolution are masked (darkened). Fault traces derived by Koukouvelas et al. (2009), Pavlidis et al. (2010) and Ganas et al. (2013).

In the area south of Pinios Lake, a significant change is observed in the direction of the trending anomalies from NNE-SSW (north) to ENE-WSW (south), near the city of Pyrgos, at the depth slices of 20 and 25 km (Figs. 10-11). This discontinuity disappears in the offshore area SSW of the town of Vartholomio, possibly marking the termination of the AFZ. A smaller anomaly lies to the NNE of the town of Andravida, where a NNE-SSW trending discontinuity between high V_P/V_S ratio values (>1.85) to the west and lower ones (<1.74) to the east can be seen at depths between 15 and 25 km (Fig. 11), where an earthquake swarm activity with magnitudes M>4.0 took place in May of 2019.

5. Discussion

Variations in seismic velocity and the V_P/V_S ratio usually depend on the rock's characteristics, such as fractures, composition, porosity, and saturation in gas or water, as well as on the rock's physical conditions, i.e., temperature and pressure (Selverstone et al. 1991; Evans and Chester 1995; Sanders et al. 1995; Faulkner et al. 2010). The orientation of P and S wave anomalies is affected both by active faults, such as Andravida Fault Zone (AFZ) and Kato Achaia normal fault (KANF), and local surface geology (Koulakov et al. 2010).

Positive NE-SW anomalies down to 25 km depth are related with the major AFZ dextral strike-slip fault (37.85º-38.12ºN, 21.40º-21.60ºE) that produced the strong (M_w6.4) earthquake of 2008 (Serpetsidaki et al., 2014). Some interesting features are revealed through the anticorrelation of V_P and V_S anomalies, with higher P and lower S velocities – resulting in high V_P/V_S ratio values (1.90-2.06). These are found to be parallel to the mean direction of mapped faults and thrusts which are mainly related to tectonic grabens. The latter are filled with a thick layer of recent sedimentary deposits so a high V_P/V_S ratio can be explained by fracturing and fluid penetration along the fault plane, as in the case of the AFZ. From Nision to Mtn. Movri in particular (Figs. 9-10), the high-velocity contrast between the western (low V_P, high V_S) and eastern (high V_P, low V_S) block of the AFZ marks a trace of the northern branch of the activated fault. Most earthquake hypocenters at these depths are in regions of relatively high velocity. The high-velocity volume overall is oriented in the SW-NE direction. The presence of high V_P/V_S ratio values at 15-20 km depth in the AFZ indicates that the rupture area consists of relatively-small-aspect–ratio, water-filled pores of the basement rock under overpressured conditions, as similar cases have shown (Takei, 2002; Nakajima et al., 2006).

In the area where the NNE-SSW anomaly bends (Mtn. Movri), the hypocentral distribution gets more involved for the depth interval between 5 and 15 km. This formation was interpreted as a branch of flower structure above a blind strike-slip fault (Zygouri et al., 2015) that caused the 2008 M_w6.4 earthquake in the lower crust of NW Peloponnese (Serpetzidaki et al., 2014). According to Halpaap et al. (2018), the aftershock sequence of the 2008 Andravida earthquake is in an area of thickened crust, where the coupling between different microplates would be a possible scenario. Sachpazi et al. (2015) attributed this structure (AFZ) to differential shear slip at the base of the Aegean crust by a similarly striking slab tearing, while Hansen et al. (2019) proposed that the AFZ plays the role of a ramp connecting the subducting segments at the Western termination of the Hellenic trench and that it is associated with the westward retreat of the oceanic slab beneath Peloponnese. Based on our result, this structure appears to be shifted southwards from Strofades to Zakynthos Islands (Figs. 9-11), extending towards the backstop of the Hellenic arc at depths between 20 and 25 km. This is probably an indication of the connection of shearing with the western part of the Ionian plate, where a major dextral flower structure – localized at the prism-backstop contact west of Zakynthos – has been deduced by Chamot-Rooke et al. (2005), and, more recently, by Gallais et al. (2011).

On the other hand, the unfractured parts of the crust are clearly expressed as high body-wave (P, S) velocity and low V_P/V_S ratio structures such as the Antirrion and Nafpaktos basins along the northern coasts of Patraikos and Western Corinth Gulf, respectively (38.35ºN, 21.75ºE), within the depth slice of 15 km. In other parts of the studied volume, a reasonably good qualitative correlation of P and S anomalies is observed. Within the depth slice of 5 km SW of Patras in particular, a WNW-ESE oriented discontinuity of positive-to-the-south (north of Mtn. Movri) and negative-to-the-north (south of the city of Patras) body-wave (P, S) velocity anomalies, is seen, coinciding with the KANF while dividing the Alpine basement of Gavrovo geotectonic and quaternary deposits, respectively. The resulting anomalies in this area are attributable to simultaneous activation of minor NW-SE trending faults in the Gulf of Patras and the ENE-WSW Agia Triada south dipping normal fault.

The results obtained in this study, in conjunction with geological observations (Koukouvelas et al., 2010; Mavroulis et al., 2013) and seismological studies (Serpetzidaki et al., 2014; Sachpazi et al., 2015; Halpaap et al., 2018; Hansen et al., 2019), provide further details for the local faults pattern in the broader area of the Western Peloponnese, offering new insights for the AFZ that was ruptured during the 2008 Andravida earthquake. The split of the AFZ into two fault branches of i) ENE-WSW and ii) NNE-SSW direction became evident in both body-wave (P, S) velocity anomalies and V_P/V_S ratio tomograms of 15 km (northern part) and 25 km (southern part), respectively. This change in the fault's orientation, combined with the complex surface tectonic structure and diffuse seismicity in the area of Mtn. Movri, support the scenario of a restraining bend of the AFZ (Fig. 12).

6. Conclusions

In this study, we performed tomographic inversion for the intricate geological and tectonic settings of the Western Peloponnese, to investigate the crustal structure in detail. The distribution of P- and S- velocity anomalies and V_P/V_S ratio are found to be consistent with the known tectonic features in the study area. This observation, in turn, corroborates the reliability of the models.

At shallower depths (5-15 km), we observed low velocities for both P- and S-waves with large V_P/V_S ratio, mainly either close to the main segments of the AFZ or in the proximity of the Quaternary basins (Patraikos Gulf). The NNE-SSW direction of such anomalies led to the highlighting of the Andravida Fault Zone (AFZ), ruptured during the 8 June 2008 earthquake (Ganas et al., 2009; Papadopoulos et al., 2010; Serpetsidaki et al., 2014). Similar values were found to be associated with major faults, which implies fracturing and fluid penetration along the plane. High-velocity structures, accompanied by low V_P/V_S ratio, were linked to unfractured parts of the crust such as the Rion-Antirrion and Nafpaktos basins.

The spatial distribution of seismic activity, body-wave (P, S) velocity anomalies, and values of V_P/V_S ratio have revealed:

- A complex shallow structure;
- The Andravida Fault Zone (AFZ) appears to be more continuous in deeper slices (at ~20 km);
- The enhanced continuity can be due to a positive flower-structure of the Andravida strike-slip fault in the area between Nision village and Mtn. Movri, as a result of a restraining bend of the AFZ.

Acknowledgments

We would like to thank Dr. Ivan Koulakov for providing the LOTOS code and his useful advice on our work, as well as the scientists, graduate students, and personnel who participated in the installation or maintenance of the stations belonging to the HUSN, and who assisted in the signal processing and manually locating the seismicity recorded. The figures were produced using ArcGIS by Esri, Surfer by Golden Software, and Generic Mapping Tools (GMT) (Wessel & Smith, 1995).

References

Aksu, A.E., Calon, T.J., Hiscott, R.N., Yasar, D. (2000) Anatomy of the North Anatolian fault zone in the Marmara Sea, western Turkey. *GSA Today* 10(6):3-7

Armijo, R., Lyon-Caen, H., Papanastassiou, D. (1992) East-west extension and Holocene normal fault scarps in the Hellenic arc. *Geology* 20:491–494

Armijo, R., Meyer, B., King, G.C.P., Rigo, A., Papanastassiou, D. (1996) Quaternary evolution of the Corinth Rift and its implications for the late Cenozoic evolution of the Aegean. *Geo Hys. J. Int.* 126:11-53

Chamot-Rooke, N., Rabaute, A., Kreemer, C. (2005) Western Mediterranean Ridge mud belt correlates with active shear strain at the prism-backstop geological contact. *Geology* 33(11):861–864

Chousianitis, K., Agalos, A., Papadimitriou, P., Lagios E., Makropoulos, K. (2010) Source parameters of moderate and strong earthquakes in the broader area of Zakynthos Island (W. Greece) from regional and teleseismic digital recordings. *Bull. Geol. Soc. Greece*, *Proc. 12th Intl. Cong.* Patras, May 2010, XLIII(4):2005-2014

Drakatos, G., Melis, N., Papanastassiou, D., Karastathis, V., Papadopoulos, G., Stavrakakis, G. (2002) 3D Crustal Velocity Structure from Inversion of Local Earthquake Data in Attiki (Central Greece) Region. *Natural Hazards* 27(N1-2):1-14

Evans, J.P., Chester, F.M. (1995) Fluid–rock interaction in faults of the San-Andreas system — inferences from San-Gabriel fault rock geochemistry and microstructures. *J. Geophys. Res. Solid Earth* 100:13007-13020

Faulkner, D.R., Lewis, A.C., Rutter, E.H. (2003) On the internal structure and mechanics of large strike-slip fault zones: field observations of the Carboneras Fault in southeastern Spain. *Tectonophysics* 367(3–4):235-251

Feredinos, G., Brooks, M., Doutsos, T. (1985) Quaternary tectonics in the Gulf of Patras, western Greece. *J. Struct. Geol.* 7(6):713–717

Gallais, F., Gutscher, M. A., Graindorge, D., Chamot-Rooke, N., Klaeschen, A.D. (2011) Miocene tectonic inversion in the Ionian Sea (central Mediterranean): Evidence from multichannel seismic data. *J. Geophys. Res.* 116:B12108

Ganas, A., Serpelloni, E., Drakatos, G., Kolligri, M., Adamis, I., Tsimi, C., Batsi, E. (2009) The M_w6.4 SW-Achaia (Western Greece) Earthquake of 8 June 2008: Seismological, field, GPS observations, and stress modeling. *J. Earthq. Eng.* 13:1101–1124

Ganas, A., Oikonomou, A.I., Tsimi, Ch. (2013) NOAFAULTS: a digital database for active faults in Greece. *Bull. Geol. Soc. Greece* XLVI

Halpaap, F., Rondenay, S., Ottemöller, L. (2018) Seismicity, Deformation and Metamorphism in the Western Hellenic Subduction Zone – New Constraints from Tomography. *J. Geophys. Res.* 123:3000–3026

Hansen, S. E., Evangelidis, C. P., Papadopoulos, G. A. (2019) Imaging slab detachment within the Western Hellenic Subduction Zone. *Geochemistry, Geophysics, Geosystems* 20:895– 912

Humphreys, E., Clayton, R.W. (1988) Adaptation of back projection tomography to seismic travel time problems. *J. Geophys. Res.* 93:1073-1085

Hollenstein, C., M. D. Müller, A. Geiger, Kahle, H.-G. (2008) Crustal motion and deformation in Greece from a decade of GPS measurements, 1993–2003. *Tectonophysics* 449:17–40

Jaxybulatov, K., Koulakov, I., Ibs-von Seht, M., Klinge, K., Reichert, C., Dahren, B., Troll, V.R. (2011) Evidence for high fluid/melt content beneath Krakatau volcano (Indonesia) from local earthquake tomography. *J. Volc. Geoth. Res.* 206(3-4):96-105

Kahle, H.-G., Muller, M.V., Geiger, A., Danuser, G., Mueller, St., Veis, G., Billiris, H., Paradissis, G. (1995) The strain field in NW Greece and the Ionian Islands; results inferred from GPS measurements. *Tectonophysics* 249:44–52

Kapetanidis, V., Papadimitriou, P., Makropoulos, K. (2010) A cross-correlation technique for relocation of seismicity in the western Corinth rift. *Bull. Geol. Soc. Greece*, *Proc. 12th Intl. Cong.* Patras, May 2010, XLIII(4):2015-2015

Kapetanidis, V., Kassaras, I. (2019) Contemporary crustal stress of the Greek region deduced from earthquake focal mechanisms. *J. Geodyn.* 123:55–82

Karakonstantis, A. (2017) *3D simulation of crust and upper mantle structure in the broader Hellenic area through Seismic Tomography*. Dissertation, National and Kapodistrian University of Athens.

Kassaras, I., Kapetanidis, V., Karakonstantis, A., Kaviris, G., Papadimitriou, P., Voulgaris, N., Makropoulos, K., Popandopoulos, G., Moshou, A. (2014) The April–June 2007 Trichonis Lake earthquake swarm (W. Greece): New implications toward the causative fault zone. *J. Geodyn.* 73:60-80

Kassaras, I., Kapetanidis, V., Karakonstantis, A. (2016) On the spatial distribution of seismicity and the 3D tectonic stress field in western Greece. *Phys. Chem. Earth, Parts A/B/C* 95:50-72

Kiratzi, A., Sokos, E., Ganas, A., Tselentis, A., Benetatos, C., Roumelioti, Z., Serpetsidaki, A., Andriopoulos, G., Galanis, O., Petrou, P. (2008) The April 2007 earthquake swarm near Lake Trichonis and implications for active tectonics in western Greece. *Tectonophysics* 452:51–65

Koukouvelas, I., Mpresiakas, A., Sokos, E., Doutsos, T. (1996) The tectonic setting and earthquake hazards of the 1993 Pyrgos earthquake, Peloponnese, Greece. *J. Geol. Soc. London* 153:39–49

Koukouvelas, I., Kokkalas, S., Xypolias, P. (2009) Surface deformation during the M_w 6.4 (8 June 2008) Movri earthquake in the Peloponnese and its implications for the seismotectonics of Western Greece. *Int. Geol. Rev*. 52(2-3):249-268

Koulakov, I. (2009) LOTOS code for local earthquake tomographic inversion. Benchmarks for testing tomographic algorithms. *Bull. Seism. Soc. Am.* 99(1):194-214

Koulakov, I., Bindi, D., Parolai, S., Grosser, H., Milkereit, C. (2010) Distribution of Seismic Velocities and Attenuation in the Crust Beneath the North Anatolian Fault (Turkey) from Local Earthquake Tomography. *Bull. Seism. Soc. Am.* 100(1):207-224

Koulakov, I., Shapiro, N. (2015) Seismic Tomography of Volcanoes. In: Beer M., Kougioumtzoglou I., Patelli E., Au IK. (Eds.) *Encyclopedia of Earthquake Engineering*. Springer.

Lagios, E., Sakkas, V., Papadimitriou, P., Damiata, B.N., Parcharidis, I., Chousianitis, K., Vassilopoulou, S. (2007) Crustal deformation in the Central Ionian Islands (Greece): Results from DGPS and DInSAR analyses (1995-2006). *Tectonophysics* 444:119-145

Lees, J.M., Crosson, R.S. (1989) Tomographic inversion for three-dimensional velocity structure at Mount St. Helens using earthquake data, *J. Geophys. Res.* 94:148-227

Lekkas, E., Fountoulis, I., Papanikolaou, D. (2000) Intensity Distribution and Neotectonic Macrostructure Pyrgos earthquake data (26 March 1993, Greece). *Natural Hazards* 21:19–33

Mavroulis, S., Fountoulis, I., Lekkas, E. (2010) Environmental effects caused by the Andravida (08-06-2008, M_L = 6.5, NW Peloponnese, Greece) earthquake. *Geologically Active: 11th IAEG Congress*, Taylor & Francis Group, Auckland, New Zealand, 451-459

Nakajima, J., Hasegawa, A., Horiuchi, S., Yoshimoto, K., Yoshida, T., Umino, N. (2006) Crustal heterogeneity around the Nagamachi-Rifu fault, northeastern Japan, as inferred from travel-time tomography. *Earth Planets Space* 58:843–853

Papadimitriou, P., Kaviris, G., Makropoulos, K. (2006) The M_w=6.3, 2003 Lefkada Earthquake (Greece) and induced transfer changes. *Tectonophysics* 423:73-82

Papadimitriou, P., Kaviris, G., Karakonstantis A., Makropoulos, K. (2010a) The Cornet seismological network: 10 years of operation, recorded seismicity and significant applications. *Ann. Geol. Pays Hell* 45:193-208

Papadimitriou, P., Agalos, A., Moshou, A., Kapetanidis, V., Karakonstantis, A., Kaviris, G., Kassaras, I., Voulgaris, N., Makropoulos, K. (2010b) An important number of recent significant earthquakes in Greece. Book of Abstracts, 32nd ESC General Assembly, Montpellier, France, 225

Papadopoulos, G.A., Karastathis, V., Kontoes, C., Charalampakis, M., Fokaefs, A., Papoutsis, I. (2010) Crustal deformation associated with east Mediterranean strike-slip earthquakes: The 8 June 2008 Movri (NW Peloponnese), Greece, earthquake (M_w6.4). *Tectonophysics* 492:201–212

Papazachos, B., Papazachou, C. (1997) *The Earthquakes of Greece*. P. Ziti & Co, Thessaloniki, Greece, 97-110

Pavlides, S., Caputo, R., Sboras, S., Chatzipetros, A., Papathanasiou, G., Valkaniotis, S. (2010) The Greek catalogue of active faults and database of seismogenic sources. *Bull. Geol. Soc. Greece* XLIII(1):486-494

Roumelioti, Z., Benetatos, C., Kiratzi, A., Stavrakakis, G., Melis, N. (2004) A study of the 2 December 2002 (M5.5) Vartholomio (western Peloponnese, Greece) earthquake and of its largest aftershocks. *Tectonophysics* 387(1-4):65–79

Sachpazi, M., Laigle, M., Charalampakis, M., Diaz, J., Kissling, E., Gesret, A., Becel, A., Flueh, E., Miles, P., Hirn, A., (2016) Segmented Hellenic slab rollback driving Aegean deformation and seismicity. *Geophys. Res. Lett.* 43:651–658

Sanders, C., Ponko, S., Nixon, L., Schwartz, E. (1995) Seismological evidence for magmatic and hydrothermal structure in Long Valley caldera from local earthquake attenuation and velocity tomography. *J. Geophys. Res.* 100:8311–8326

Selverstone, J., Morteani G., Staude, J.M. (1991) Fluid channeling during ductile shearing: transformation of granodiorite into aluminous schist in the Tauern Window, Eastern Alps. *J. Metamorph. Geol.* 9:419-431

Serpetsidaki, A., Elias, P., Ilieva, M., Bernard, P., Briole, P., Deschamps, A., Lambotte, S., Lyon-Caen, H., Sokos, E., Tselentis, G.A. (2014) New constraints from seismology and geodesy on the M_w = 6.4 2008 Movri (Greece) earthquake: evidence for a growing strike-slip fault system. *Geophys. J. Int.* 198 (3):1373–1386

Takei, Y. (2002) Effect of pore geometry on V_P/V_S: From equilibrium geometry to crack. *J. Geophys. Res.* 107(B2):2043

Toomey, D.R., Foulger, G.R. (1989) Tomographic inversion of local earthquake data from the Hengill-Grensdalur Central Volcano Complex, Iceland. *J. Geophys. Res.* 94(B12):17497–17510

Tselentis G.-A. (1998) Fault lengths during the Patras 1993 earthquake sequence as estimated from the pulse width of initial P wave. *Pure Appl. Geophys.* 152(1):75-89

Wessel, P., Smith, W.H.F. (1995) New version of the Generic Mapping Tools released. *EOS Trans. AGU* 76:329

Zygouri, V., Koukouvelas, I.K., Kokkalas, S., Xypolias, P., Papadopoulos, G.A. (2015) The Nisi Fault as a key structure for understanding the active deformation of the NW Peloponnese, Greece. *Geomorph.* 237:142–156